Supplementary Material for "Linear Transforms for Fourier Data on the Sphere: Application to High Angular Resolution Diffusion MRI of the Brain"

Justin P. Haldar*, Richard M. Leahy

Signal and Image Processing Institute, Ming Hsieh Department of Electrical Engineering, University of Southern California, Los Angeles, CA, USA

This supplement contains additional material to complement the results presented in the main body of the paper. The material presented here uses the same definitions, variables, and acronyms that were introduced therein.

1. Effects of fractional anisotropy and ξ on the FRACT

Two-tensor simulations were also performed to demonstrate the characteristics of FRACT for tensors with a range of different anisotropy characteristics, and for a range of different ξ values. As in the previous simulations, we generated data using a linear combination of two diffusion tensor models with $\lambda_1 > \lambda_2 = \lambda_3$, and both tensor components were given the same relative volume fraction. The principal tensor orientations were separated by 60°, and the mean diffusivity of both tensors was set to 700×10^{-6} mm^2/s. The tensor eigenvalues were adjusted to achieve fractional anisotropies between 0 and 1. The simulated acquisition used a b-value of 2000 s/mm^2 and $N = 256$. Results of applying the FRACT to this data are shown in Fig. S1. As can be seen, as the simulated diffusion tensors become more isotropic (i.e., fractional anisotropy decreases), the reconstructed FRACT ODFs shrink in magnitude, which is expected because the FRACT nullifies the isotropic components of the diffusion signal. This feature makes it easy to discriminate between isotropic and anisotropic diffusion characteristics. In addition, the figure confirms that FRACT results vary smoothly as a function of ξ.

2. Effects of Harmonic Order on the FRACT and FRT

Complementing Figs. 9-11 from the main paper, we also performed similar simulations to examine the effects of the maximum spherical harmonic degree L on the performance of the FRACT and the FRT. These results are shown in Fig. S2. We found that performance for both transforms is relatively insensitive to L when $L \geq 8$, as expected from the analysis in the previous section. It should be noted that while larger values of L correspond to increasingly ill-posed least-squares estimation problems for the spherical harmonic coefficients of $E(\mathbf{q})$, the stabilizing effect of the Laplace-Beltrami regularization seems to mitigate any potential resulting noise amplification effects.

3. Effects of SNR and N on the FRACT and FRT

Complementing Fig. 11 from the main paper, we also performed similar experiments with $N = 64$. These results are shown in Figs. S3, and have very similar characteristics to the results shown in Fig. 11 for $N = 256$, other than a small increase in the variance of the histogram peaks as N decreases. Given the theoretical analysis (e.g., Figs. 5 and 6 from the main paper), it is not surprising that $N = 64$ and $N = 256$ have similar resolution characteristics. However, it is notable that increasing N does not have a more significant impact on the low-SNR results, since increasing N might be expected to have an effect similar to averaging. The lack of more substantial improvement with increasing N can be attributed to the signal bias introduced by the noise floor of the Rician signal distribution (which will not diminish with increasing N), which reduces diffusion contrast between dominant and non-dominant diffusion directions, hence negatively impacting the ability to accurately identify fiber orientations.

4. Effects of Volume Fraction on the FRACT and FRT

The numerical simulations presented in the main paper used multi-tensor signal models, where each tensor component had the same relative volume fraction. A natural question is how FRACT would behave if the volume fraction were to vary. Due to the fact that both the FRACT and FRT are linear transforms, the theory would suggest that the FRACT/FRT ODFs for a multi-tensor model should simply be the linear combination of the FRACT/FRT ODFs for the individual tensors, weighted by the relative volume fraction of each tensor component. To test this, additional simulations were performed using the same simulation setup as in Figs. 9-11 from the main paper, but allowing the volume fraction to vary. Results of these simulations are shown in Fig. S4.

It should be noted that the min-max normalization that is used for visualization purposes nonlinearly modifies the appearance of the ODFs in a manner that can potentially confound a

*Corresponding author at: 3740 S. McClintock Avenue, EEB #442 M/C 2564, Los Angeles, CA 90089-2564, USA. Tel.: +1 213 740 2458; fax +1 213 740 4651.

Email addresses: jhaldar@usc.edu (Justin P. Haldar), leahy@sipi.usc.edu (Richard M. Leahy)

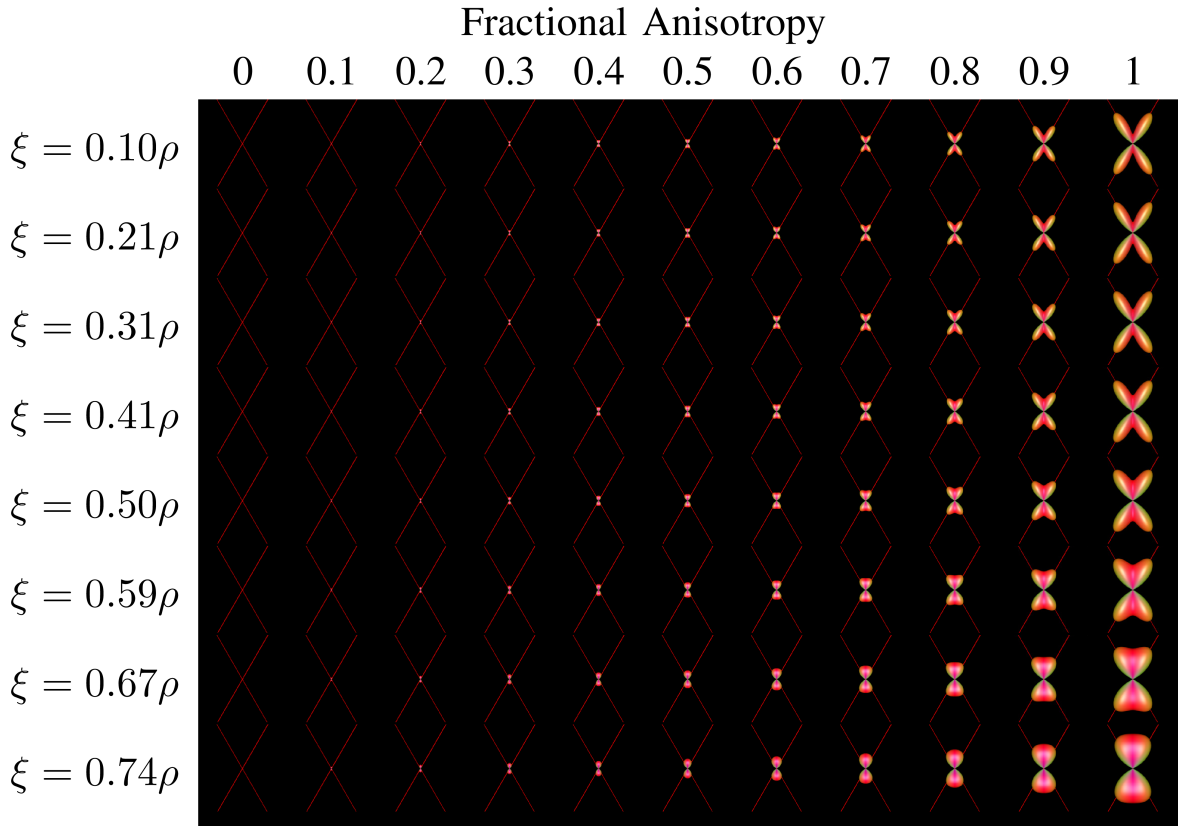

Figure S1: Results of applying the FRACT to a two-tensor simulation for various values of the tensor fractional anisotropy and ξ. The lines shown in each image correspond to the principal directions of the two tensors used for simulation. Unlike the figures in the main paper, the reconstructed ODFs in this figure are not normalized to illustrate their relative "size."

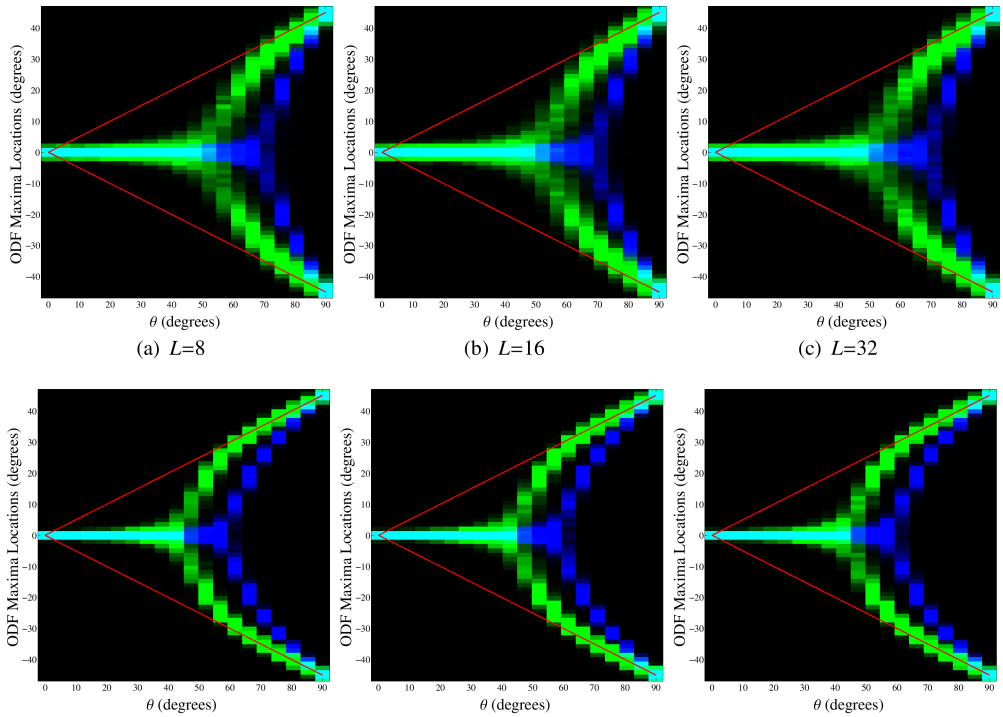

(a) L=8 (b) L=16 (c) L=32

(d) L=8 (e) L=16 (f) L=32

Figure S2: Histograms for the locations of local maxima extracted from the FRT profiles (in blue) and the FRACT profiles (in green) as a function of the true angular separation between two simulated tensors. The color scale is set to saturate at 250 counts in a single histogram bin for improved visualization. The true orientations of the two tensors are also indicated using red lines. All simulations used SNR=80, $\xi = 0.34\rho$, and $N = 256$. The images from left to right show results for different values of L. Results are shown for (a)-(d) a b-value of 1000 s/mm^2 and (e)-(h) a b-value of 2000 s/mm^2.

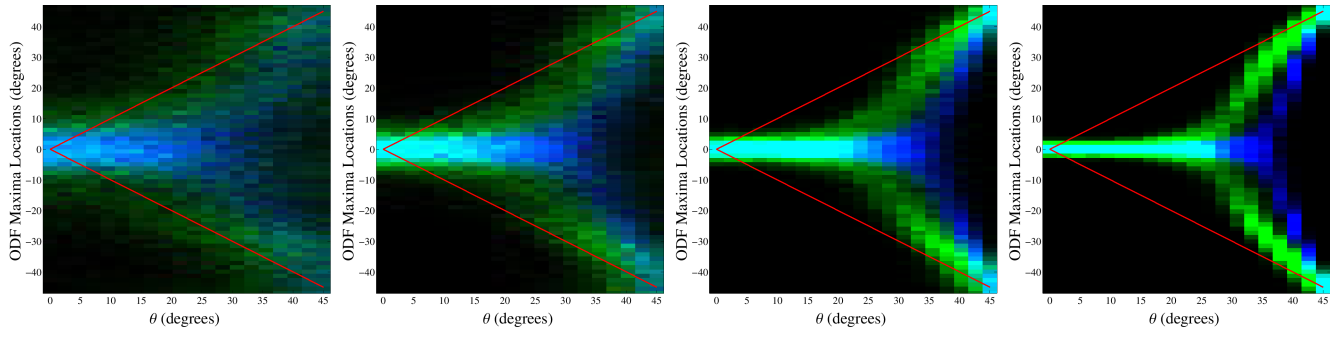

(a) SNR=10 (b) SNR=20 (c) SNR=40 (d) SNR=80

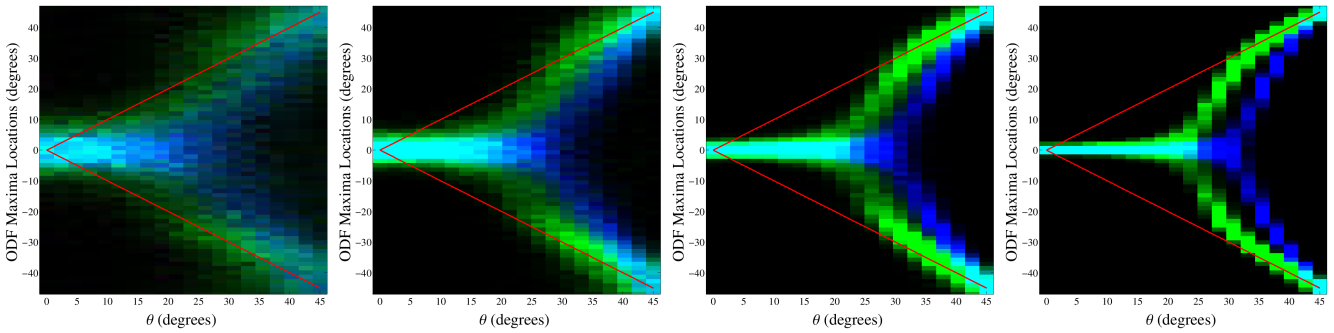

(e) SNR=10 (f) SNR=20 (g) SNR=40 (h) SNR=80

Figure S3: Histograms for the locations of local maxima extracted from the FRT profiles (in blue) and the FRACT profiles (in green) for two simulated tensors in the x-y plane with orientation angles of $-\theta$ and $+\theta$ in polar coordinates. The color scale is set to saturate at 250 counts in a single histogram bin for improved visualization. The true orientations of the two tensors are also indicated using red lines. All simulations used $\xi = 0.34\rho$, $N = 64$, and $L = 8$. The images from left to right show results for different SNRs. Results are shown for (a)-(d) a b-value of 1000 s/mm^2 and (e)-(h) a b-value of 2000 s/mm^2.

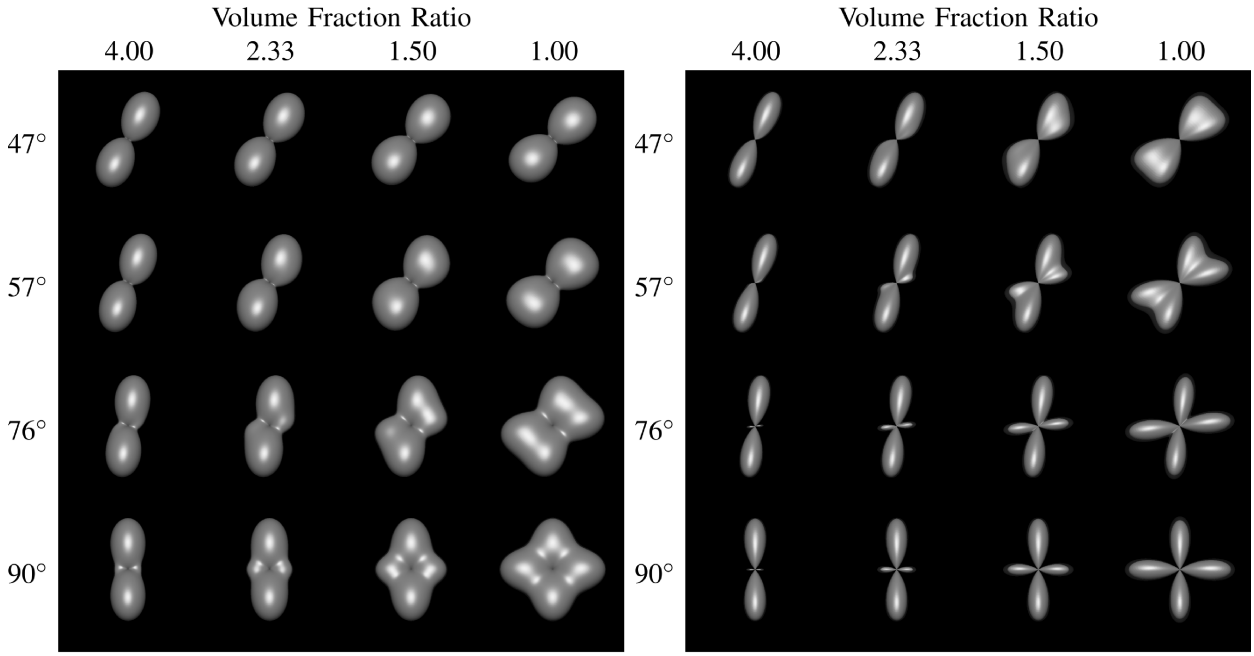

(a) FRT (b) FRACT

Figure S4: The impact of the volume fraction ratio (horizontal axis) on the (a) FRT and (b) FRACT in multi-tensor simulations with varying fiber crossing angles (vertical axis). All simulations used $N = 256$, $L = 8$, SNR=80, and a b-value of 2000 s/mm^2.

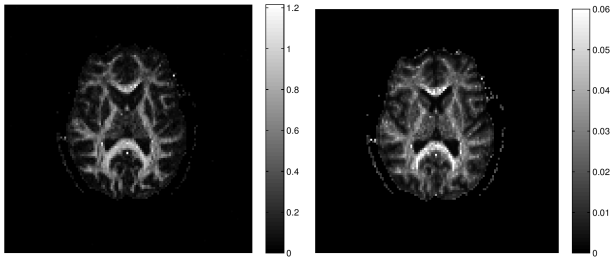

(a) Fractional Anisotropy (b) Norm of FRACT ODF

Figure S5: (a) Conventional fractional anisotropy computed from a diffusion tensor model of real brain data. (b) Euclidean norm of the FRACT ODF for the same data.

visual assessment of the relative volume fraction of each component. However, as expected, the multi-tensor ODFs are almost identical to a weighted linear combination of ODFs based on single tensors, with any variations resulting from the small amount of simulated noise that was used in the simulations. It is observed that angular resolution capabilities are generally better when the different tensor components have similar volume fractions. When the volume fraction ratios are very different, there is a tendency for the smaller ODF peaks to be hidden in the "side-bands" of the dominant ODF peak. Note that these angular resolution characteristics are not specific to the FRT and FRACT, but would also be found with the other ODF estimation approaches that have been proposed for this kind of data. Angular partial volume effects will also confound the ability to accurately estimate volume fractions from the values of the FRT and FRACT ODF peaks, unless additional modeling constraints are imposed (e.g., the fiber response modeling used in constrained spherical deconvolution).

5. Novel Measures of Anisotropy?

Tissue anisotropy measures have been widely used in diffusion MRI to characterize biological tissues. Since the FRACT is a method that provides an ODF estimate, any ODF-based anisotropy measures can also be used with the FRACT. However, one of the characteristics of the FRACT is that it nullifies isotropic components of the diffusion signal. One of the anonymous reviewers suggested that this property could be used to enable novel FRACT-specific methods for measuring the anisotropy of different tissues. To examine the feasibility of this idea, we computed the Euclidean norm of the FRACT ODF, which can be performed efficiently by taking the square-root of the sum-of-squares of the spherical harmonic coefficients of the FRACT ODF. The results of this are shown in relation to the DTI-based fractional anisotropy measure in Fig. S5. As can be seen, variations in this FRACT-based measure reflect real variations in brain tissue characteristics. The measure has large similarities to conventional fractional anisotropy, though some differences in the spatial distribution of the measure are also apparent. This measure (or similar variations) could potentially be used in quantitative studies to provide novel insight into the tissue characteristics of different subjects. However, we should also caution that the physical interpretation of this measure is not entirely clear, and that the measure is lacking in both units and normalization. Further adjustments and/or extensive additional testing would be necessary to prove the utility of such measures for practical applications, particularly given the large number of ways to quantify anisotropy that have previously been proposed in the literature.